# Passive Stability of a Spinning Skylab

S. M. SELTZER*
*NASA George C. Marshall Space Flight Center, Ala.*

**An analytical investigation is made of the rotational dynamics of a torque-free rigid body which must spin about a principal axis of intermediate moment of inertia. Massless flexible booms with discrete tip masses are attached to the body, and the physical characteristics of these appendages are determined so that the rotational dynamics of the composite body will be stable. The parameter plane stability technique is applied to linearized equations of motion representing the model with the physical characteristics of a spinning Skylab. The transient response to external disturbances is predicted in terms of appendage characteristics and vehicle spin rate and then calculated explicitly in a design example.**

## Nomenclature

$a_p$ = coefficients of wobble characteristic equation ($p$ ranges from 0–4)
$d_i = 2m\zeta_i\omega_{n_i}$ = structural damping coefficient in $i$ direction
$E$ = unit matrix of same dimensions as $F$ matrix
$F$ = matrix associated with vector matrix state equation $x' = Fx$
$I_i^*$ = principal moment of inertia of rigid-core body about $i$ body-fixed coordinate
$I_1, I_2, I_3$ = principal moment of inertia of body about $i$ coordinate $I_1^* + 2m\Gamma^2$, $I_2^*$, $I_3^* + 2m\Gamma^2$, respectively
$K_1, K_2$ = ratios of inertia $(I_2 - I_3)/I_1$ and $(I_3 - I_1)/I_2$, respectively
$k_i$ = stiffness coefficient characterizing non-rotating boom stiffness
$\mathcal{L}^{-1}$ = inverse Laplace transform
$m$ = tip mass of boom
$T_i$ = applied torque about $i$ coordinate
$t$ = time
$u_i = u_i^1 - u_i^2$ = skew symmetric mode of elastic deformation
$u_i^m$ = displacement of $m$ tip mass from spinning steady state in $i$ direction ($m = 1, 2$)
$w_i$ = perturbation (about spinning steady state) velocity about $i$ coordinate
$X_p, Y_p$ = real and imaginary parts of $\lambda^p$, respectively
$\mathbf{x}(\tau) = [w_1, w_2, \mu_3, \mu_3']^T$ = wobble-motion state vector
$\alpha$ = a positive constant such that $k_2 = \alpha k_1$
$\Gamma$ = steady-state boom dimension in 2-axis direction from center of mass to tip mass
$\gamma_i = 2m\Gamma^2/I_i$ = dimensionless inertia ratio
$\Delta_i = d_i/m\Omega$ = dimensionless damping ratio
$\zeta_i = \eta/(\nu^2 + \eta^2)^{1/2}$ = damping ratio of boom in $i$ direction
$\lambda = s/\Omega = \eta + i\nu$ = normalized Laplace operator
$\mu_i = u_i/2\Gamma$ = generalized skew symmetric coordinate
$\nu_n = (\nu^2 + \eta^2)^{1/2}$ = nondimensional natural frequency
$\sigma_i^2 = k_i/m\Omega^2$ = dimensionless natural frequency coefficient of boom
$\tau = \Omega t$ = dimensionless time
$\Phi(\tau)$ = state transition matrix
$\Phi_{qr}$ = elements of state transition matrix
$\Omega$ = steady-state spin rate about 3 axis
$\boldsymbol{\omega} = [w_1, w_2, \Omega + w_3]^T$ = angular velocity vector
$\omega n_i$ = natural frequency of boom in $i$ direction
$()'$ = differentiation with respect to $\tau$

*Subscript*

$i$ = index referring to three body-fixed coordinates ($i = 1, 2, 3$)

Received February 28, 1972; revision received May 11, 1972. A portion of this paper was presented at the IEEE Region III Conference, Chatanooga, Tenn. April 10–12, 1972. The author gratefully acknowledges the advice of J. Patel, Principal Engineer with Teledyne-Brown Engineering Company, Huntsville, Ala.

Index categories: Manned Space Station Systems; Spacecraft Attitude Dynamics and Control.

* Senior Research Scientist, Astrionics Laboratory. Associate Fellow AIAA.

## Introduction

IF it should be desired to provide artificial gravity by spinning the Skylab, the solar panels still must point toward the sun. The vehicle would be required to spin about a principal axis of intermediate moment of inertia, which cannot be done stably. That axis can be made the axis of maximum moment of inertia by deploying masses on the tips of extendable booms in a direction perpendicular to the spin axis. A simplified model of the modified spinning Skylab is described, and analyses of the stability of motion and the rotational dynamics are presented.

## Model Definition and Equations of Motion

The geometrically complex Skylab[1] (Fig. 1) is simplified to make it analytically tractable. The vehicle is modeled (Fig. 2) as a single rigid-core body with principal moments of inertia $I_i^*$ with $I_1^* < I_3^* < I_2^*$. Attached to the core body are two flexible massless booms, each of length $\Gamma$ and each having a tip mass $m$. In the steady state, the principal moments of inertia of the entire vehicle coincide with the body-fixed axes and are designated $I_i$ with $I_1 < I_2 < I_3$. The vehicle is assumed to have a steady-state spin velocity $\Omega$ about the 3 axis, and the angular velocity vector is written in body-fixed coordinates as $\boldsymbol{\omega} = [w_1, w_2, \Omega + w_3]^T$ where $w_i$ represents small perturbations about the steady state—i.e.,

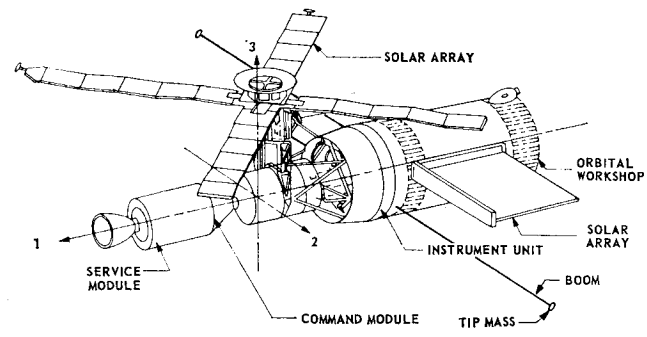


Fig. 1 Skylab.

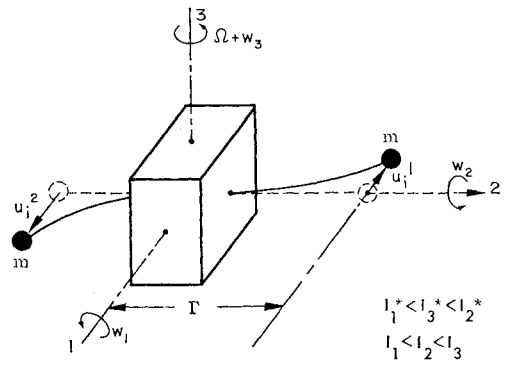


**Fig. 2 Simplified model.**

$|w_i| \ll \Omega$. Displacements $u_i^m (m = 1, 2)$ of the tip masses from the spinning steady state are assumed to be small. Nonrotating boom stiffness is characterized by stiffness coefficients $k_i$. Structural damping is assumed proportional to elastic deformation velocities and is denoted by coefficients $d_i$. Rotational dynamics of the vehicle may be represented by a set of nine differential equations written in variables $u_i^m$, $w_i$. The set may be reduced to six by making the substitution $u_i = u_i^1 - u_i^2$ where $u_i$ represents the skew symmetric mode of the elastic deformations, and hence causes angular motion about the vehicle's steady-state attitude. In this investigation, stability of rotational motion is of interest, so only the skew symmetric mode will be considered. The corresponding linearized equations of motion are

$$w_1' - K_1 w_2 + \gamma_1 \Omega(\mu_3'' + \mu_3) = T_1/I_1\Omega$$
$$w_2' - K_2 w_1 = T_2/I_2\Omega$$
$$(1/\Omega)(w_1' + w_2) + \mu_3'' + \Delta_3\mu_3' + (\sigma_3^2 + 1)\mu_3 = 0 \quad (1)$$

and

$$w_3' - \gamma_3\Omega(\mu_1'' - 2\mu_2') = T_3/I_3\Omega$$
$$(-1/\Omega)w_3' + \mu_1'' + \Delta_1\mu_1' + \sigma_1^2\mu_1 - 2\mu_2' = 0$$
$$(-2/\Omega)w_3 + 2\mu_1' + \mu_2'' + \Delta_2\mu_2' + (\sigma_2^2 - 1)\mu_2 = 0 \quad (2)$$

For physical reasons $|K_j| < 1 (j = 1, 2), 0 < \gamma_j < 1 (j = 1, 3)$, $d_i > 0$, and $k_i > 0$. Equations (1) describe wobble motion (resulting from angular motions about the 1 and 2 axes and linear motion in the 3 direction). Equations (2) describe in-plane motion (a combination of angular motion about the 3 axis and linear motions in the 1 and 2 directions).

## Stability Analysis

The motion of the vehicle can be described by a nutation about the axis of angular momentum which, in the absence of external torques, is inertially fixed. This motion is called passively stable if the nutation damps out and the vehicle rotates only about the axis of angular momentum (the effect of applied torques $T_i$ is to change the attitude of this axis). The following analysis determines under what conditions the spinning vehicle can be passively stabilized, assuming $I_1 < I_2 < I_3$.

The stability of wobble motion is investigated by obtaining the characteristic equation from Eqs. (1)

$$(1 - \gamma_1)\lambda^4 + \Delta_3\lambda^3 - (K_1K_2 + \gamma_1K_2 + \gamma_1 - \sigma_3^2 - 1)\lambda^2$$
$$- \Delta_3 K_1K_2\lambda - [(\sigma_3^2 + 1)K_1K_2 + \gamma_1K_2] = 0 \quad (3)$$

Regions of stability may be determined by applying the *D*-composition technique.[2] The stability boundary associated with the origin of the complex $\lambda$-plane is found by setting the coefficient of $\lambda^0$ equal to zero in Eq. (3), yielding

$$K_2 = -[(\sigma_3^2 + 1)/\gamma_1]K_1K_2 \quad (4)$$

The boundary associated with infinity on the $\lambda$-plane is found by setting the coefficient of $\lambda^4$ equal to zero

$$\gamma_1 = 1 \quad (5)$$

The stability boundary associated with the imaginary axis of the $\lambda$-plane is found by setting $\lambda$ equal to $i\nu$ in Eq. (3), and writing the real and imaginary parts of the result as the two equations

$$[\nu^2 - (\sigma_3^2 + 1)]K_1K_2 + \gamma_1(\nu^2 - 1)K_2$$
$$= -\nu^2[(1 - \gamma_1)\nu^2 + (\gamma_1 - \sigma_3^2 - 1)]$$

and

$$-\Delta_3\nu(K_1K_2 + \nu^2) = 0 \quad (6)$$

Eqs. (6) may be solved for the relationship

$$K_2 = -K_1K_2 \quad (7)$$

Finally, a stability boundary may exist that is associated with the singular case where Eqs. (6) are not independent—i.e., when the Jacobian $J$ becomes identically equal to zero[2]. The Jacobian of Eqs. (6) is

$$J = \Delta_3\gamma_1\nu(\nu^2 - 1) \quad (8)$$

which is zero when $\Delta_3$, $\gamma_1$, or $\nu$ equals zero, or when $\nu^2 = 1$. If $\nu^2 = 1$ is substituted into Eqs. (6), the $J = 0$ stability boundary is found as

$$K_1K_2 = -1 \quad (9)$$

These stability results corroborate those reported by Barbera.[3]

The wobble-motion stability requirements may be portrayed on a $K_1K_2$, $K_2$ parameter plane (Fig. 3). The stable region may be found by considering the sign of $J$.[2] Double cross-hatching is used on the boundary associated with the imaginary axis (including the $J = 0$ boundary). The hatching lies on the side of the boundary that is toward the stable region; in the $\lambda$-plane, it lies on the left side of the boundary for increasing $\nu$. If $J > 0$, the hatching in the parameter plane will also lie on the left side of the boundary as $\nu$ increases (and on the right side if $J < 0$). Single cross-hatching is used similarly on the boundary associated with the origin of the $\lambda$-plane. Continuity of cross-hatching must exist at contour intersections in the parameter plane corresponding to the origin of the $\lambda$-plane and to other intersections where the contours have equal values of $\nu$.

The effect of boom flexibility on stability may be assessed by considering the booms to be rigid; i.e., setting $1/\sigma_i^2$ equal to zero. The boundary of Eq. (4) becomes $K_1K_2 = 0$. The stable region is thus decreased by boom flexibility, as shown

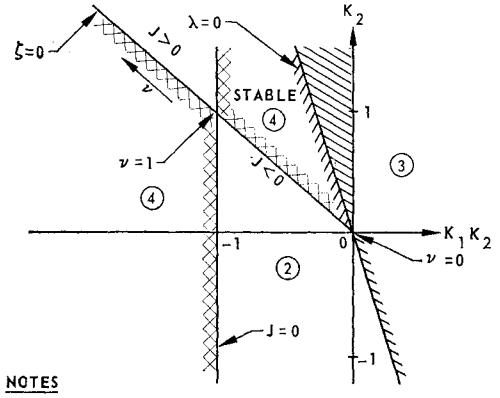


**Fig. 3 Stability region for wobble motion.**

by the shaded region of Fig. 3. Also, the effect of boom length and tip mass may be seen by considering their effect on $K_1$.

Similarly, stability of the in-plane motion may be determined by examining the characteristic equation obtained from Eqs. (2)

$$\lambda\{(1-\gamma_3)\lambda^4 + [\Delta_1 + \Delta_2(1-\gamma_3)]\lambda^3 + [\sigma_1^2 + \sigma_2^2(1-\gamma_3) + 3(1-\gamma_3) + \Delta_1\Delta_2]\lambda^2 + [\Delta_1(\sigma_2^2 - 1 + 4\gamma_3) + \Delta_2\sigma_1^2]\lambda + \sigma_1^2(\sigma_2^2 - 1 + 4\gamma_3)\} = 0 \quad (10)$$

If it is assumed that the stiffness coefficient $k_2$ is $\alpha$ times as great as $k_1$ and $k_3$, where $\alpha$ is a positive constant, $1/\alpha \ll 1$, and that $\zeta_1 = \zeta_3$, the application of $D$-composition to Eq. (10) yields the boundary associated with the origin of the $\lambda$-plane

$$\sigma_2^2 = 0 \text{ and } \sigma_2^2 = 1 - 4\gamma_3 \quad (11)$$

The boundary associated with infinity on the $\lambda$-plane is $\gamma_3 = 1$. The boundary associated with the imaginary axis of the $\lambda$-plane yields the same two boundaries plus an additional constraint, $\Delta_2 = 0$. No additional boundaries arise from the $J = 0$ condition. The resulting region of stability is shown on a $\gamma_3$, $\sigma_2^2$ parameter plane (Fig. 4), which shows the effects of the boom characteristics on the stability of the in-plane motion.

## Wobble-Motion Dynamics

Once stability has been assured, the transient dynamics of the wobble motion are of interest. The character of this motion may be investigated by using the parameter plane technique.[2] From the parameters in characteristic equation (3), inertia ratios $K_1K_2$ and $K_2$ are selected as two adjustable parameters of interest to the designer—i.e., the effect of various values of $K_1K_2$ and $K_2$ on the wobble-motion dynamics will be determined. This is done by finding the relationship between these two parameters and the roots of Eq. (3). The relationship may be shown by mapping a convenient contour from the $\lambda$-plane onto the $K_1K_2$, $K_2$ parameter plane. The contour selected is the line

$$\lambda = -\zeta\nu_n + i\nu_n(1-\zeta^2)^{1/2} \quad (12)$$

where $\nu_n = \nu(1-\zeta^2)^{-1/2}$. Any root of Eq. (3) lying on this contour will have a specified damping ratio $\zeta$. This line is mapped onto the parameter plane by substituting Eq. (12) into Eq. (3), which may be written in the form

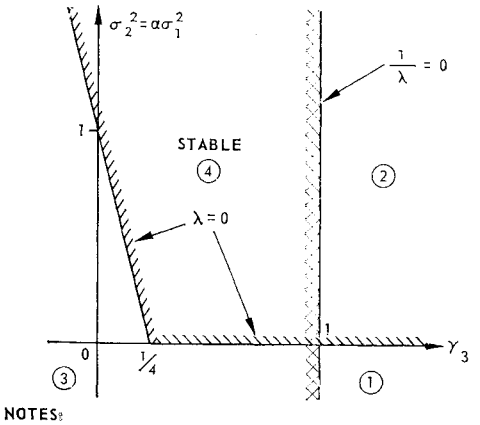


NOTES:
1. SEE NOTE 2, FIG. 3
2. ADDITIONAL CONSTRAINT: $\Delta_2 > 0$

**Fig. 4 Stability region for in-plane motion.**

$$\sum_{p=0}^{4}(a_pK_1K_2 + b_pK_2 + c_p)\lambda^p = 0 \quad (13)$$

where values for coefficients $a_p$, $b_p$, $c_p$ are found in Table 1. If $\lambda^p$ is written as the sum of its real and imaginary parts,

$$\lambda^p = X_p + iY_p \quad (14)$$

values of $X_p$ and $Y_p$ may be found from the recurrence formulas,

$$X_{p+1} + 2\zeta\nu_nX_p + \nu_n^2X_{p-1} = 0$$
$$Y_{p+1} + 2\zeta\nu_nY_p + \nu_n^2Y_{p-1} = 0 \quad (15)$$

where it is seen from Eqs. (12) and (14) that $X_0 = 1$, $Y_0 = 0$, $X_1 = -\zeta\nu_n$, and $Y_1 = \nu_n(1-\zeta^2)^{1/2}$. Substituting Eq. (14) into Eq. (13) and separating the resulting real and imaginary parts, one obtains two simultaneous algebraic equations that may be solved for parameters $K_1K_2$ and $K_2$

$$K_1K_2 = (B_1C_2 - B_2C_1)/J, \quad K_2 = (A_2C_1 - A_1C_2)/J$$
$$J = A_1B_2 - A_2B_1 \quad (16)$$

where

$$A_1 = \sum_{p=0}^{4}a_pX_p, \quad B_1 = \sum_{p=0}^{4}b_pX_p, \quad C_1 = \sum_{p=0}^{4}c_pX_p$$

and

$$A_2 = \sum_{p=0}^{4}a_pY_p, \quad B_2 = \sum_{p=0}^{4}b_pY_p, \quad C_2 = \sum_{p=0}^{4}c_pY_p \quad (17)$$

Equations (16) define the parameter plane contour corresponding to Eq. (12) in the $\lambda$-plane for a chosen value of $\zeta$ and coefficients $a_p$, $b_p$, $c_p$. Each contour is plotted as a function of the nondimensional natural frequency $\nu_n$.

The real roots of the system may also be mapped from the $\lambda$-plane onto the parameter plane. Each selected value $\eta$ of a real root is substituted for $\lambda$ in characteristic Eq. (13). The resulting equation will define a contour on the parameter plane representing the selected location $\eta$ of the real root.

The response of the system in terms of variables $w_1$, $w_2$, $\mu_3$ may be found by casting Eqs. (1) in the form

$$\mathbf{x}' = F\mathbf{x} \quad (18)$$

where the vector $\mathbf{x}$ is defined as

$$\mathbf{x} = [w_1, w_2, \mu_3, \mu_3']^T \quad (19)$$

and the matrix $F$ is

$$F = \frac{1}{(1-\gamma_1)} \cdot \begin{bmatrix} 0 & (\gamma_1 + K_1) & \gamma_1\sigma_3^2 & \gamma_1\Delta_3 \\ K_2(1-\gamma_1) & 0 & 0 & 0 \\ 0 & 0 & 0 & (1-\gamma_1) \\ 0 & -(K_1+1) & (\gamma_1 - \sigma_3^2 - 1) & -\Delta_3 \end{bmatrix} \quad (20)$$

The response $\mathbf{x}(\tau)$ may then be found from

$$\mathbf{x}(\tau) = \Phi(\tau)\mathbf{x}(0) \quad (21)$$

where $\mathbf{x}(0)$ is the initial condition vector and $\Phi(\tau)$ is the state transition matrix

**Table 1 Coefficients of wobble; characteristic equation**

| $p$ | $a_p$ | $b_p$ | $c_p$ |
|---|---|---|---|
| 0 | $-(\sigma_3^2 + 1)$ | $-\gamma_1$ | 0 |
| 1 | $-\Delta_3$ | 0 | 0 |
| 2 | $-1$ | $-\gamma_1$ | $1 + \sigma_3^2 - \gamma_1$ |
| 3 | 0 | 0 | $\Delta_3$ |
| 4 | 0 | 0 | $1 - \gamma_1$ |

$$\Phi(\tau) = e^{F\tau} = \mathcal{L}^{-1}\{[\lambda E - F]^{-1}\} \tag{22}$$

In evaluating $\Phi(\tau)$, the roots of the characteristic equation (3) are the roots of the determinant $|\lambda E - F|$ and may be taken directly from the parameter plane (for example, if initial conditions exist only on $w_1$ and $w_2$—i.e.

$$\mathbf{x}(0) = [x_{10}, x_{20}, 0, 0]^T \tag{23}$$

the $w_1(\tau)$ response is found from

$$w_1(\tau) = \mathcal{L}^{-1}[\Phi_{11}(\lambda)x_{10} + \Phi_{21}(\lambda)x_{20}] \tag{24}$$

where

$$\Phi_{11}(\lambda) = \lambda[\lambda^2 + \Delta_3\lambda/(1-\gamma_1) + (1+\sigma_3{}^2-\gamma_1)/(1-\gamma_1)]/|\lambda E - F|$$
$$\Phi_{21}(\lambda) = K_2\Phi_{11}(\lambda)/\lambda \tag{25}$$

## Example

The model described by Eqs. (1) and (2) is used to represent a spinning Skylab. Representative values for the coefficients in Eq. (3) are given in Table 2. If the values are substituted into Eqs. (16), $\zeta$-contours may be plotted on the $K_1K_2$, $K_2$ parameter plane as functions of $\nu_n$ (Fig. 5). Stability boundaries defined by Eqs. (4, 7, and 9) are also plotted in Fig. 5. Real root boundaries are found to be outside the stable region and hence are of no interest in the Skylab problem.

**Table 2 Physical characteristics of Skylab**

| | | |
|---|---|---|
| $I_1{}^* = 1.01 \times 10^6$ kg m$^2$ | $\Gamma = 23.3$ m | $k_2 = 7.4 \times 10^4$ N/m |
| $I_2{}^* = 6.90 \times 10^6$ kg m$^2$ | $m = 227$ kg | $d_i = 0.04(k_i\text{m})^{1/2}$ |
| $I_3{}^* = 6.85 \times 10^6$ kg m$^2$ | $k_1 = k_3 = 146$ N/m | $\Omega = 0.6\ s^{-1}$ |

A typical design point for Skylab is shown on the parameter plane. It corresponds to the physical characteristics shown in Table 2. The corresponding roots of the characteristic equation are seen to have damping ratios $\zeta$ and nondimensional natural frequencies $\nu_n$ of

$$\zeta = 0.002, \quad \nu_n = 0.2854$$

and

$$\zeta = 0.01863, \quad \nu_n = 1.7612 \tag{26}$$

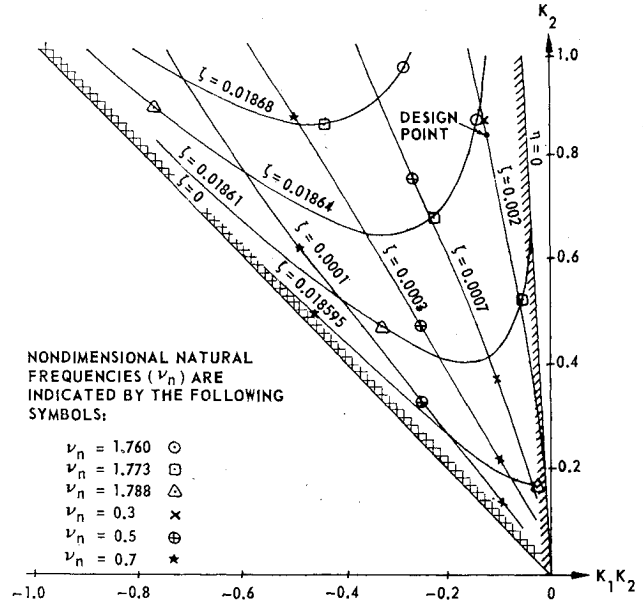


Fig. 5 $K_2$ vs $K_1K_2$ parameter plane plot.

If the values of Table 2 and Eqs. (26) are substituted into Eq. (21), the response for the Skylab model is found. For example, from Eq. (24)

$$w_1(\tau) = 1.0978e^{-0.0005672\tau}\cos(0.2854\tau + 0.3274)w_1(0) + 0.09359e^{-0.03281\tau}\cos(1.761\tau + 4.1270)w_2(0) \tag{27}$$

For $w_1(0) = w_2(0) = 0.001$, the response $w_1(\tau)$ is plotted in Fig. 6. Similarly, $w_2(\tau)$ and $\mu_3(\tau)$ are also determined and shown in Figs. 7 and 8.

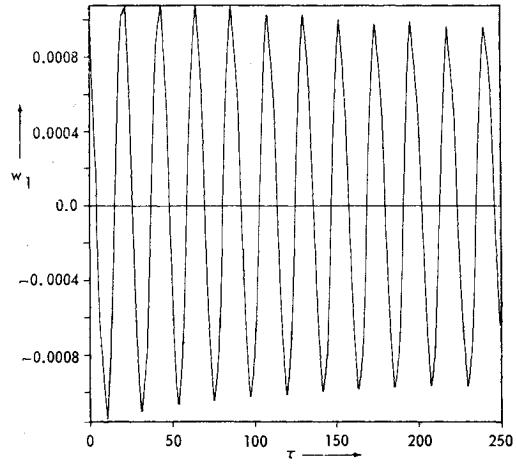


Fig. 6 $w_1$ vs $\tau$.

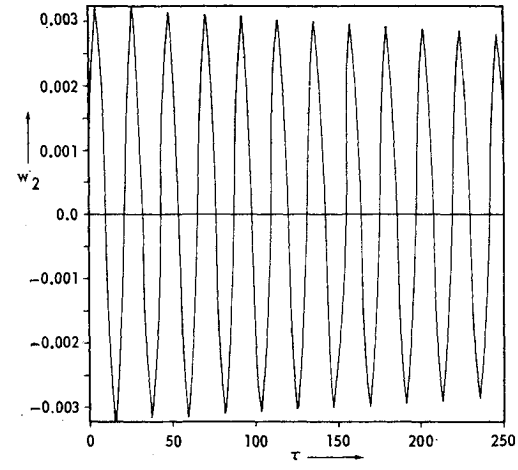


Fig. 7 $w_2$ vs $\tau$.

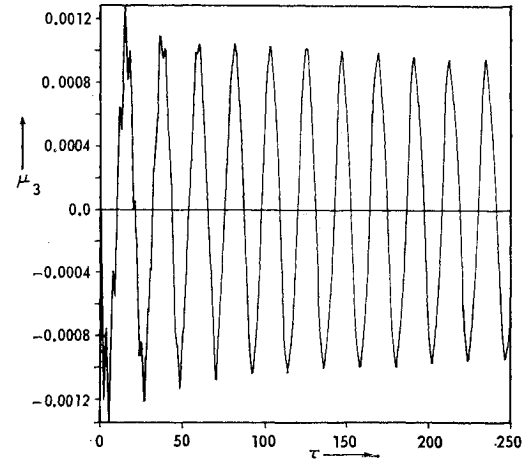


Fig. 8 $\mu_3$ vs $\tau$.

## Conclusion

It has been shown that it is possible to stabilize passively the motion of a simplified model of a spinning Skylab by deploying flexible booms, thus altering the moments of inertia. Analytical results indicate the required boom-stiffness properties for given vehicle mass properties and spin rates to achieve passive stability. Furthermore, the use of the simplified model leads to results amenable to physical interpretation.

To gain confidence that these results will apply to the actual Skylab, an additional step is being implemented. A detailed digital simulation model of the spinning Skylab vehicle has been developed at the Marshall Space Fight Center, and results compare favorably with those of the simplified model.

## References

[1] Chubb, W. B. and Seltzer, S. M., "Skylab Attitude and Pointing Control System", TND-6068, 1971, NASA.

[2] Siljak, D. D., *Nonlinear Systems*, Wiley, New York, 1969, pp. 4–51, 33–37, 404–406, and 455–457.

[3] Barbera, F. J., "Attitude Stability of Spinning Flexible Spacecraft," Ph.D. dissertation, 1971, Univ. of California, Los Angeles, Calif.

SEPTEMBER 1972 J. SPACECRAFT VOL. 9, NO. 9

# Supersonic Dynamic Stability Experiments on the Space Shuttle

K. J. ORLIK-RÜCKEMANN*, J. G. LABERGE† AND E. S. HANFF†
*National Aeronautical Establishment,‡ Ottawa, Ontario, Canada*

**A wind-tunnel study was performed of the longitudinal dynamic stability of the shuttle spacecraft at supersonic speeds. In particular, the study included the determination of the damping-in-pitch characteristics of the orbiter and of the booster, both separately and in a mated launch configuration, and the investigation of the effect of a simulated rocket exhaust plume and of the static and dynamic interference during abort separation. Static interference is defined here as caused by the proximity of the second vehicle when that vehicle is stationary, whereas dynamic interference denotes the same effect, but with the other vehicle performing an oscillatory motion. It was found that, in general, the static interference effects were small, whereas, for the case of the orbiter and the booster performing synchronous oscillations, the dynamic interference effect was very large and could lead to a strongly negative damping of the orbiter.**

## Introduction

THE unconventional configurations employed for the space shuttle and its often rather unusual flight conditions render the analytical prediction of its aerodynamic characteristics extremely difficult. Thus in many cases the experimental data constitute the sole source of information. One such area where a heavy dependence on experiments is necessary involves the prediction of the dynamic stability characteristics of the shuttle. Although often not of critical importance for the preliminary design, this information usually is required for the complete performance analysis. In addition, there are several flight conditions, such as the ascent of the launch configuration, some phases of the abort separation, and the transitional flight of the orbiter, where the dynamic stability characteristics of the shuttle may very well prove to be significant in the final design and formulation of operational procedures.

This paper describes the dynamic stability experiments on the shuttle, which were performed as part of the internal research program of the National Aeronautical Establishment (NAE). In addition to discussing certain new concepts and new techniques which were specially developed for these experiments, the paper contains a representative selection of dynamic stability results for the shuttle, including certain unusual interference effects such as those occurring during an abort separation and in the presence of an exhaust plume. Oil-flow visualization pictures and high-speed shadowgraph movies are used to illustrate some of the complex flowfields involved in these cases.

Presented as Paper 72-135 at the AIAA 10th Aerospace Sciences Meeting, San Diego, Calif., January 17–19, 1972; submitted January 19, 1972; revision received May 3, 1972.

Index categories: Aircraft Handling, Stability and Control; Aircraft and Component Wind Tunnel Testing.

* Head, Unsteady Aerodynamics Laboratory. Associate Fellow AIAA.

† Research Officers.

‡ A division of the National Research Council of Canada.

## Experimental Arrangement

The experiments were performed on 1/360 scale models of the fully reusable shuttle spacecraft, which were manufactured and supplied by NASA Langley Research Center. Models typical of both the low cross-range and the high cross-range configurations were investigated. The former were represented by a straight-wing orbiter and a straight-wing booster, and the latter by a delta-wing orbiter and swept-wing canard booster. Details of the two sets of models are given in Refs. 1–3. The pitching moment derivatives of both orbiters were referred to the total wing area and the wing mean aerodynamic chord, while a scaled-down standard reference area (10,000 ft$^2$) and reference length (200 ft) were used for the two boosters. The distance of the axis of oscillation (and the moment reference point) from the model nose, referred to the model length, was 0.612 and 0.610 for the straight-wing orbiter and booster, respectively, and 0.456 and 0.465 for the delta-wing orbiter and booster.